DOI 10.4430/bgo00372

Kernel based regularisation parameter and source dependent depth weighting in gravity data inversion

R. Varfinezhad and V.E. Ardestani

Institute of Geophysics, University of Tehran, Iran

(Received: 27 April 2021; accepted: 2 August 2021; published online: 14 February 2022)

ABSTRACT In this paper, an inversion algorithm for gravity data is presented. The algorithm exploits a model weighting matrix derived from multiplication of compactness and the modified depth weighting, with its exponent being dependent on the source type. Regularisation parameter and the exponent of depth weighting are the critical inverse parameters: the first is adopted according to the maximum value of the kernel matrice (MaxKer) and the second takes the value of the structural index associated with the source type of interest. The productivity of the proposed method is examined through three synthetic and two real data sets. According to the derived results from synthetic examples, the optimised value found for the regularisation parameter to successfully invert the perfect and noisy data sets are 10^{-7}×MaxKer and 10^{-1}×MaxKer, respectively. Ultimately, we manipulate the inversion algorithm on the two real data sets, from the: i) salt dome of Rogun in Tajikistan and ii) Safo manganese mine in Iran. The suggested value for the regularisation parameter in real cases is 0.05×MaxKer, which is close to the corresponding value to invert the noise contaminated data. Since source types for both cases were known from *a priori* information, 2 is attributed to the exponent of depth weighting.

Key words: compactness, depth weighting, gravity, inversion, regularisation parameter, kernel.

1. Introduction

The gravity method has been applied for different practical applications such as tectonic studies (Linsser, 1967; Paterson and Reeves, 1985), mineral investigation (Paterson and Reeves, 1985; Vatankhah *et al*., 2014), oil-gas explorations (Nettleton, 1976), and also in engineering and environmental surveys (Hinze, 1990; Ward, 1990). Different kinds of ambiguities, such as theoretical ambiguity due to the Gauss theorem, sampling ambiguity because of the insufficiency of discrete data to represent the gravity field perfectly and algebraic ambiguity due to more unknowns than observations, need confronting when we are dealing with gravity data inversion. Furthermore, data are contaminated by the noise leading to instability of the inverse solution. Therefore, using constraints such as compactness, depth weighting, smoothness, minimisation of inertia momentum, and others are required in order to remove these problems and find a realistic and stable solution. It should be noted that disparate combinations of these constraints lead to different algorithms; each of them can be efficient, depending on the case (Varfinezhad *et al*., 2020).

Last and Kubic (1983) introduced a compactness function, minimising the volume of the anomaly in 3D inversion schemes (area in 2D). Reconstructed anomalies from compactness algorithm are too extensive horizontally and for some cases, the retrieved anomaly remains too shallow. Hence, Guillen and Menichetti (1984) broadened this technique by manipulating the constraint of minimising moment of inertia with respect to the centre of gravity or with respect to a given dip line passing through it. Applying this method results in more compact and deeper anomalies. Barbosa and Silva (1994) extended the compact gravity inversion technique by incorporating *a priori* information about the maximum compactness of the anomalous sources along several axes. This generalised compact gravity inversion procedure can work successfully for constant, linear density sources such as mineralisation along faults. Li and Oldenburg (1996) presented an algorithm for a 3D inversion of magnetic data, and the same for a 3D inversion of gravity data (Li and Oldenburg, 1998). The objective function consists of two terms: data misfit and model objective function, which allows introducing *a priori* information using one or more weighting functions. Their main innovation was related to incorporating a depth weighting function in the algorithm. Pilkington (1997) utilised depth weighting and smoothness constraints in the model weighting objective function. The author used the conjugate gradient to solve the inverse problem due to the very large number of model parameters involved in the reconstruction procedure. Portniaguine and Zhadanov (1999) presented a stabilising functional called minimum gradient support (MGS) producing more focused inversion images compared with other conventional stabilisers like smoothness or total variation. Boulanger and Chouteau (2001) combined compactness, depth weighting, smoothness, and hardness constraints using a Lagrangian formulation. *A priori* information on density and allowed density ranges were also included in the inversion scheme. Pilkington (2009) inserted sparseness and depth weighting into the model objective function. He solved the inversion procedure in data space using a conjugate gradient and showed that solving the problem in data space leads to a much more focused image compared with the inversion model solved in model space. Namaki *et al*. (2011) presented a 2D blocky inversion scheme for which a multiterm cost function based on edge-preserving penalty functions were optimised. This method was applied on long airborne magnetic flight data in SE Iran. Cella and Fedi (2012) updated the depth weighting function introduced by Li and Oldenberg (1996, 1998) through assigning structural index value of the anomaly to the exponent of the depth weighting and they showed the effectiveness of this modified depth weighting function by utilising different synthetic and real data sets. A self-constrained inversion method was proposed by Paoletti *et al*. (2013), implemented in two steps: i) source parameters such as the horizontal position of the source body edges, the structural index, source depth to the top, are estimated, ii) then, these pieces of *a priori* information are introduced in the objective function as depth and spatial weighting constraints. Ialongo *et al*. (2014) have demonstrated that invariant and realistic source-distribution models are acquired by employing the same depth weighting exponent for the potential fields and for their *k*-order derivatives. More papers can be found in literature about gravity data inversion (e.g. Vatankhah *et al*., 2014; Meng *et al*., 2017).

In this paper, a simple, but efficient inversion algorithm is presented which includes a compactness constraint and the modified depth weighting function introduced by Cella and Fedi (2012). Multiplication of these well-known constraints are implemented as weighting matrix in the weighted minimum length solution which is different from the other proposed methods. Another main originality of this paper is to adopt a regularisation parameter according to the maximum value of kernel matrix, whereas L-curve and generalised cross validation (GCV) are two widespread techniques for this purpose. The efficiency of the suggested inversion algorithm will be shown through different synthetic and real data cases.

2. Methodology

2.1. Forward modelling

For 2D gravity modelling, considering the subsurface of the interested area is discretised into a lot of prismatic cells infinitely elongated in strike direction (here *y* direction) and assuming constant density contrast for each cell (Fig. 1), the forward response of the anomaly can be computed by the following formula:

$$d_i = \sum_{j=1}^{M} A_{ij} m_j + e_i \qquad i = 1.2. \ldots . N \tag{1}$$

d_i is *i*th calculated data, A_{ij} is an element of kernel matrix (forward operator) representing the *j*th cell effect on *i*th data, m_j is density contrast of *j*th cell and e_i is *i*th element of the added noise vector to the data.

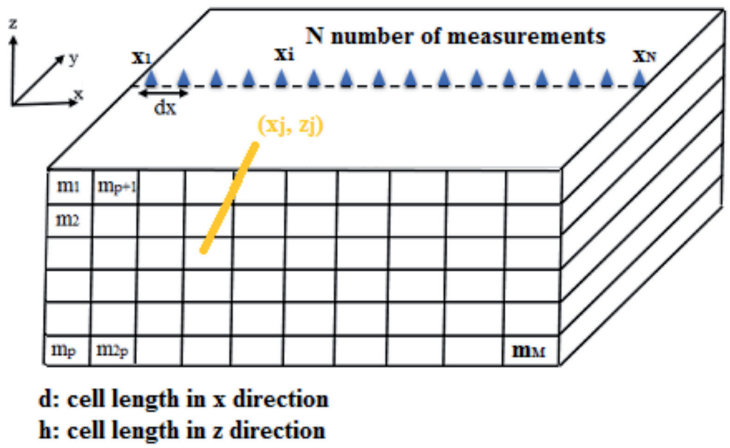

Fig. 1 - Discretisation of the subsurface into infinitely elongated prismatic cells along strike direction (here *y* coordinate). Number of measurements and model parameters are *N* and *M*, respectively.

A_{ij} elements can be obtained according to the following equation (Last and Kubic, 1983):

$$A_{ij} = 2\gamma[\left(x_i - x_j + \frac{d}{2}\right) log\left({}^{r_2 r_3}/_{r_1 r_4}\right) + d\ log\left({}^{r_4}/_{r_3}\right) - \left(z_j + \frac{h}{2}\right)(\theta_4 - \theta_2) + \left(z_j - \frac{h}{2}\right)(\theta_3 - \theta_1)] \tag{2}$$

y is gravitational constant and *r* and ϑ may be calculated as (Last and Kubic, 1983):

$$r_1^2 = (z_j - \frac{h}{2})^2 + (x_i - x_j + \frac{d}{2})^2 \qquad \theta_1 = \arctan(x_i - x_j + \frac{d}{2})/(z_j - \frac{h}{2})$$

$$r_2^2 = (z_j + \frac{h}{2})^2 + (x_i - x_j + \frac{d}{2})^2 \qquad \theta_2 = \arctan(x_i - x_j + \frac{d}{2})/(z_j + \frac{h}{2})$$

$$r_3^2 = (z_j - \frac{h}{2})^2 + (x_i - x_j - \frac{d}{2})^2 \qquad \theta_3 = \arctan(x_i - x_j - \frac{d}{2})/(z_j - \frac{h}{2})$$

$$r_4^2 = (z_j + \frac{h}{2})^2 + (x_i - x_j - \frac{d}{2})^2 \qquad \theta_4 = \arctan(x_i - x_j - \frac{d}{2})/(z_j + \frac{h}{2})$$

Eq. 2 allows us to calculate the gravity response for a given model.

2.2. Inversion

In the inversion process, we seek a density contrast distribution relative to a reference model so that its forward response fits the observed data with an acceptable misfit error. Because of the non-uniqueness and instability of the inversion solution, as mentioned above, introducing constraints such as a model weighting matrix and a regularisation term are required. In order to solve the linear system of Eq. 1, the following objective function is minimised (Tikhonov and Arsenin, 1977):

$$\min \rightarrow \ \|W_d(Am - d)\|_2^2 + \alpha\|W_m(m - m_r)\|_2^2 \tag{3}$$

where m_r is the reference model, α is regularisation parameter and W_d and W_m are data and model weighting matrices, respectively. In all synthetic and real cases here, m_r is assumed to be zero and $W_d = I$. Solving Eq. 3 can lead to the following weighted damped minimum length solution (e.g. Menke, 2012):

$$m = m_r + (W_m^{-1}A^T)(AW_m^{-1}A^T + \alpha W_d)^{-1}(d - Am_r) \tag{4}$$

W_m is the model weighting matrix derived from multiplication of compactness and depth weighting functions. The compactness constraint introduced by Last and Kubic is defined as (Last and Kubic, 1983):

$$W_c = \frac{1}{(m + \varepsilon)^2} \tag{5}$$

where m is the model parameter vector and ε is a very small value preventing the denominator being zero. The depth weighting matrix was introduced for the first time by Li and Oldenberg (1996):

$$W_z = \frac{1}{(Z)^{(\beta/2)}} \tag{6}$$

where Z and β are the vectors of cell centre coordinates and the depth weighting exponent, respectively. Suggested β values for magnetic and gravity methods were 3 and 2, respectively, by Li and Oldenburg (1996, 1998). Cella and Fedi (2012) attributed the structural value, which may be obtained by methods such as Euler deconvolution or DEXP (Fedi, 2007), to the depth weighting exponent, therefore, the range of β values for gravity case is from 2 to -1 (Table 1). Here, we exploit this modified flexible depth weighting function. An important issue that should be clarified is the difference between our algorithm and those proposed by Portniaguine and Zhadanov (1999, 2002):

1) compactness constraint uses m-$m_{apriori}$ while in the focusing algorithm (Portniaguine and Zhadanov, 1999) ∇m, which means the gradient of the vector of model parameters, is utilised. In an iteration cycle, if $m_{apriori}$ considered to be equal to $m_{k\text{-}1}$, then both compactness and focusing constraints coincide. Here, we use a reference model instead of $m_{apriori}$, which is assumed to be zero model during iteration cycle, therefore, there is a clear difference between compactness and focusing stabilisers. Furthermore, in the focusing algorithm (Portniaguine and Zhadanov, 1999), depth weighting is not manipulated by the authors;
2) Portniaguine and Zhadanov (2002) take advantage of compactness and sensitivity constraints which play the role of depth weighting but it is worth mentioning that we use the modified depth weighting function introduced by Cella and Fedi (2012) and this makes our algorithm significantly different;
3) an important originality found in our algorithm is related to the regularisation parameter adoption, which is chosen depending on the maximum value of the kernel matrix and its efficiency will be demonstrated by different synthetic and real cases.

Table 1 - Structural indices (magnetic and gravity methods) for different types of one-point source to which the depth estimation refers (Reid *et al*., 1990; Stavrev, 1997; Reid, 2003; FitzGerald *et al*., 2004; Cella and Fedi, 2012).

Source type	N (Magnetic)	N (Gravity)	Depth relative to
Sphere	3	2	Centre
Vertical cylinder	2	1	Top
Horizontal cylinder	2	1	Centre
Dyke	1	0	Top
Sill	1	0	Centre
Contact	0	-1	Top

Because of the dependence of the weighting matrix to model m the inversion procedure is iterative. Acquiring the model needs the following steps:

i) for the first iteration, the compactness matrix is assumed to be an identity matrix and Eq. 3 is solved,
ii) lower and upper bounds are applied on the obtained model parameters,
iii) compactness and then the updated model weighting matrix is computed from the obtained inverse model for the next iteration and Eq. 3 is again solved,
iv) this process is continued until the interested misfit between measured data and calculated data from the inversion result is satisfied or improvement in the inversion model from one iteration to the next iteration is not significant so that $\frac{m_i^{k+1}-m_i^k}{m_i^k} < 0.02$, $i = 1, \ldots, M$, where M is the number of model parameters and k is the kth iteration number.

3. Synthetic modelling

The inversion algorithm is then applied to the different synthetic cases to investigate its efficiency and address the determination of the regularisation parameter according to the maximum value of the kernel matrix. Furthermore, these examples will be indicative of the efficiency of the modified depth weighting function introduced by Cella and Fedi (2012).

3.1. Blocks in different depths

For the first synthetic case, a block anomaly in a homogenous background with different depths to top (10, 30, and 60 m) is considered, whose density contrast relative to the background is 1000 kg/m^3 (1 g/cm^3) (Fig. 2a). Block extensions in horizontal and vertical directions are 40 and 30 m, respectively. Forward responses of these models are illustrated in Fig. 2b. Data are corrupted to the normally distributed random noise with level of 2% of the maximum value of

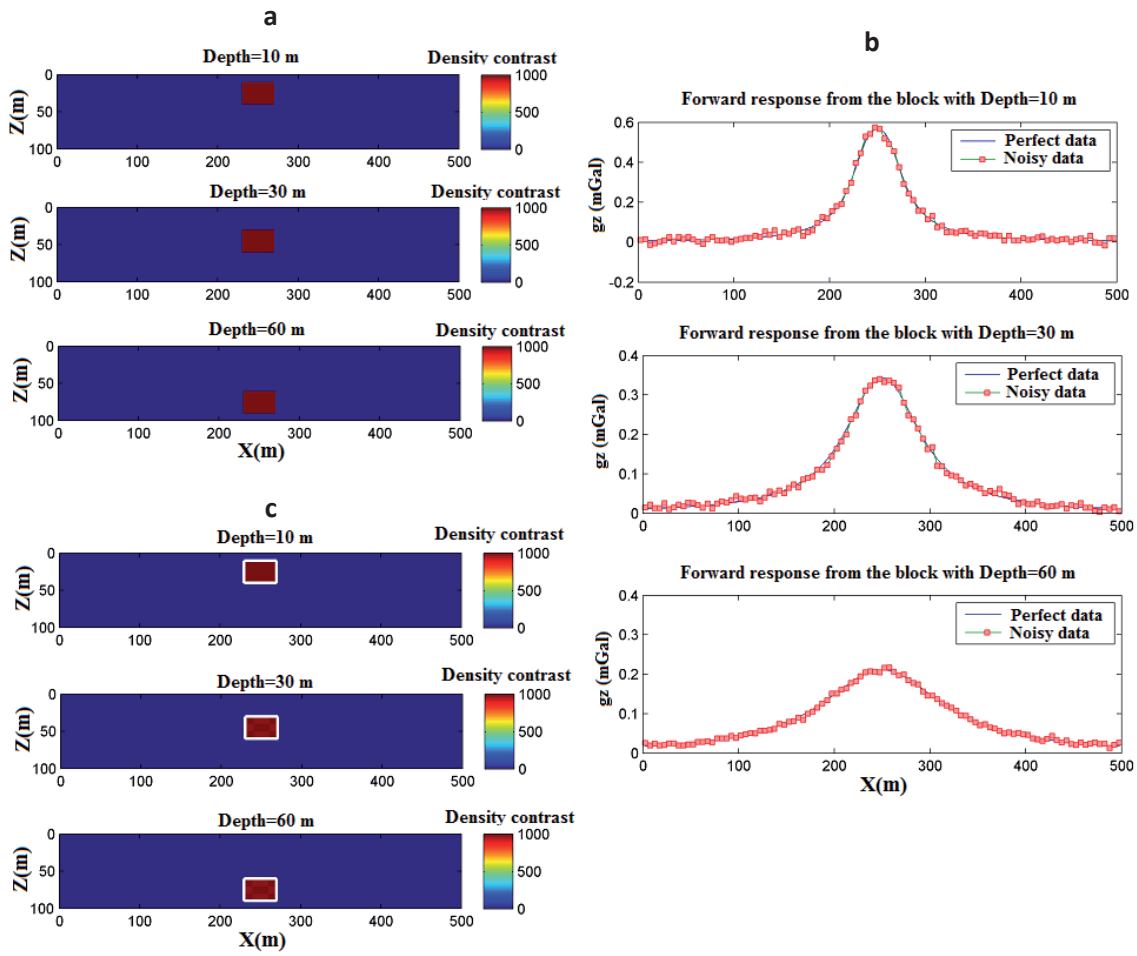

Fig. 2 - a) True model of a block in a homogenous background with different depths at 10, 30, and 60 m. b) Forward responses of the block models in panel A without noise and when they are corrupted by the noise with the level of 2%. c) Inversion results from the noise-free data derived by the adopted algorithm and demonstrating the perfect rendering of a true model for all three cases. Density contrast is in kg/m^3.

the data vector (Fig. 2b). Reconstructed models for noise-free and noisy cases are represented in Figs. 2c and 3, respectively. As can be observed in Fig. 2c, the algorithm can retrieve the blocks in different depths perfectly for noise free data. The regularisation parameter, depth weighting exponent, number of iterations and rms errors of data misfit for all cases, can be found in Table 2, suggesting that the regularisation parameter can be chosen according to the maximum value of the kernel matrix (MaxKer). For all the block models, a regularisation parameter of 10^{-7}×MaxKer proves to be an appropriate value. Depth weighting exponent of 2 is selected for all of them as proposed by Cella and Fedi (2012), indicating that the exponent depends on the source type.

This instructive and simple example has two important features: i) with the fixed exponent of 2, block models with different depth ranges can be recovered very well and we do not need to change the depth weighting exponent for anomalies in different depths, ii) the regularisation parameter for noise-free data inversion can be adopted according to the maximum value of the kernel and the value 10^{-7}×MaxKer is enough to lead to the promising results. The following different synthetic examples also certify these important notes. The number of iterations for the deepest case is 8 and it is different from the two other ones, which are 4, probably because of being the deepest anomaly. For noise corrupted data, the reconstructed models are shown in Fig. 3.

Table 2 - Inversion parameters for noise-free data. Maximum value of the kernel matrix is 2.1688×10^{-4}.

Block model	Regularisation parameter	Depth weighting exponent	Number of iterations	Rms (%)
Depth = 10 m	10^{-7}×MaxKer	2	4	0.02
Depth = 30 m	10^{-7}×MaxKer	2	7	0.1
Depth = 60 m	10^{-7}×MaxKer	2	8	0.14

The regularisation parameter is enlarged significantly to 10^{-1}×MaxKer for all cases to obviate instability of the solution in the presence of random noise, while depth weighting exponent and number of iterations are fixed to 2 and 6, respectively (Table 3). In the next different synthetic case, the performance of the inverse algorithm is probed to see that these choices for the inverse parameters work.

Table 3 - Inversion parameters for noisy data with the level of 2%. Maximum value of the kernel matrix is 2.1688×10^{-4}.

Block model	Regularisation parameter	Depth weighting exponent	Number of iterations	Rms (%)
Depth = 10 m	10^{-1}×MaxKer	2	6	2.79
Depth = 30 m	10^{-1}×MaxKer	2	6	2.50
Depth = 60 m	10^{-1}×MaxKer	2	6	1.28

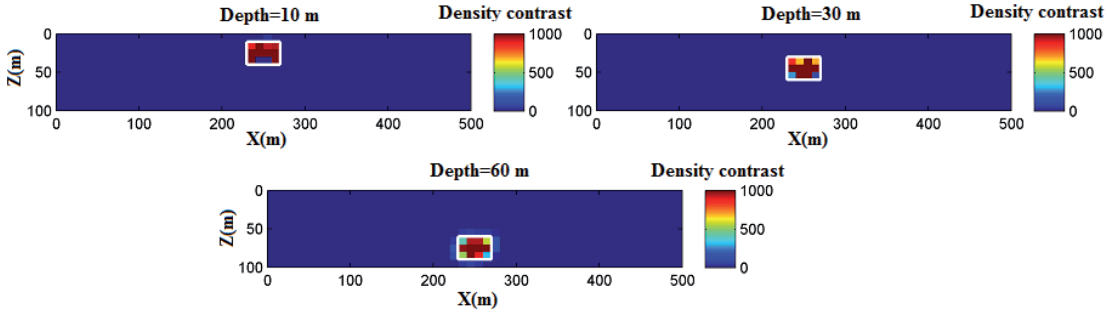

Fig. 3 - Inverted models from 2% noisy data for the block models situated in three different depths at 10, 30, and 60 m. For all three cases, the regularisation parameter, depth weighting exponent, and number of iterations are 10^{-1}×MaxKer, 2, and 6, respectively. Density contrast is in kg/m^3.

3.2. Vertical dyke

The second synthetic model is a vertical thin dyke with the depth to top of 20 m and it is extended to the depth of 100 m. The dyke thickness and its density contrast relative to the background are 10 m and 1000 kg/m^3, respectively. The dyke model and its forward response can be observed in Fig. 4A. Fig. 4B represents the inversion results from noise free data and noise corrupted data as the previous synthetic example (normally distributed noise with level of 2%). The retrieved model from noise-free data is demonstrative of the perfect rendering of the true model. The reconstructed dyke model from noise contaminated data shows good agreement with boundaries of the true dyke model, but recovered density contrast involves some errors, which can be expected due to the presence of noise on the data. Adopted inversion parameter values can be found in Table 4. According to the modified depth weighting function by Cella and Fedi (2012), 1 is attributed to the depth weighting exponent and inversion results derived from perfect and noisy data sets are indicative of the appropriateness of this value for the vertical dyke case. For noise-free data and noise contaminated data, regularisation parameters are the same as the case of the block model, which is another certification allowing us to choose this parameter according to the maximum value of the kernel and it is not required to change the regularisation parameter value. For both cases, the number of iterations is 8 implying no significant difference with the previous synthetic example. Finally, it can be concluded that a high level of similarity can be found between this synthetic example with the previous one about choosing the main inversion parameters.

Table 4 - Inversion parameters for the vertical thin dyke model.

Dyke model	Regularisation parameter	Depth weighting exponent	Number of iterations	Rms (%)
Noise free data	10^{-7}×MaxKer	1	8	0.39
Noisy data (2%)	10^{-1}×MaxKer	1	8	5.18

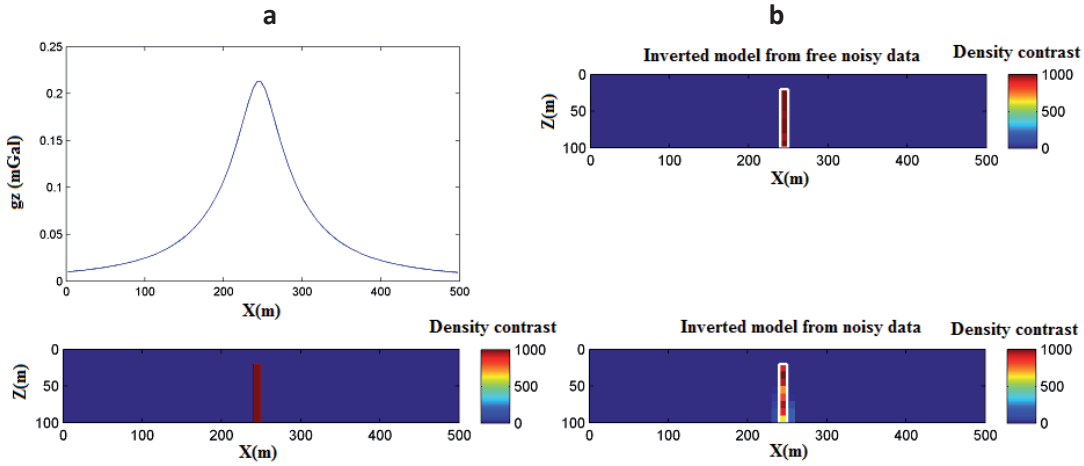

Fig. 4 - a) True model of the vertical dyke and its corresponding forward response. b) Inversion models from noise-free and noise contaminated data. The reconstructed model from noise free data, as the previous synthetic example, results in the perfect rendering of the true model, while in the presence of noise there are some differences between recovered density contrast (kg/m^3) relative to the true value.

3.3. Multisource model

The third synthetic case considered here is a multisource model where all of the sources are disparate in various aspects such as horizontal and vertical extensions, the depth to the top of the anomalies and density contrasts relative to the background (Fig. 5a). Since all of them are block type bodies, which have a very similar shape to a sphere rather than the others that can be found in Table 1, they are assigned the structural index of 2. Table 5 expresses the characteristics of these three sources. Retrieved models of noise free and noisy data are represented in Fig. 5b. The retrieved model from noise-free data represents a good rendering of the shallowest anomaly with respect to its spatial extension and density contrast, while noise contaminated data inversion leads to the thinner body with a depth to the top estimation error of 5 m. For the second anomaly from the right side, the noise-free data inversion results in an anomaly whose depth to top is in agreement with the true body, but there is an error in its depth to the bottom. Furthermore, except the central part, the density contrast of the block at the top and lower part has a disparate value in comparison with the true amount. Inversion of noisy data for this second anomaly, contains errors on the estimation of the depth to the top and bottom of the anomaly. Variation of recovered density contrast along the upper and lower boundary of this anomaly is evident. For the deepest block, inversion of noise-free and noisy data leads to roughly similar results, but it can be stated that the upper part of the anomaly derived from noise free data represents greater similarity with the true anomaly. It should also be mentioned that the density contrasts of the inverted model have differences with true models along the anomaly boundaries. Moreover, in spite of being the deepest anomaly, the discrepancy between the results of noise free data and noisy data is not as much as the two other blocks. This issue can be justified since this block produces a larger gravity anomaly (data) in the surface and we added the random noise with the level of 2% of the maximum value of the data vector to the perfect data. Therefore, this noise produces larger relative random changes on the observed anomalies corresponding to the other two blocks (second and third peaks of observed data curve from left in Fig. 5c) and consequently, larger errors can be observed in the reconstruction of these two blocks in the inversion process of noisy data. Table 6 shows the

adopted values for the regularisation parameter, depth weighting exponent, number of iterations and misfit rms errors of the computed data. The values of this table are also consistent with the previous ones for selecting the regularisation parameter and source-type dependent exponent of depth weighing function. Number of iterations is 4 and they are less than 10 as usual for synthetic examples.

Concerning these synthetic cases, an important issue remains to be addressed. In order to have a desirable inversion model from 2% noisy data, the regularisation parameter was greatly increased from 10^{-7} to 10^{-1} (6 orders of magnitude) which shows the high sensitivity of gravity data inversion to the random noise, but does not mean that the presented inversion algorithm is not robust and efficient for noisy data, but rather that only a very large change in the regularisation parameter relative to the cases of inverting perfect data is required. In addition, the practical efficiency of the presented algorithm will be demonstrated using two different real cases in the following section.

Table 5 - Characteristics of bock anomalies for the multisource case.

Source	Horizontal extension (m)	Vertical extension (m)	Depth to the top (m)	Density contrast (kg/m³)
Block 1	100-160	40-80	40	1500
Block 2	230-270	30-70	30	1000
Block 3	380-420	20-50	20	750

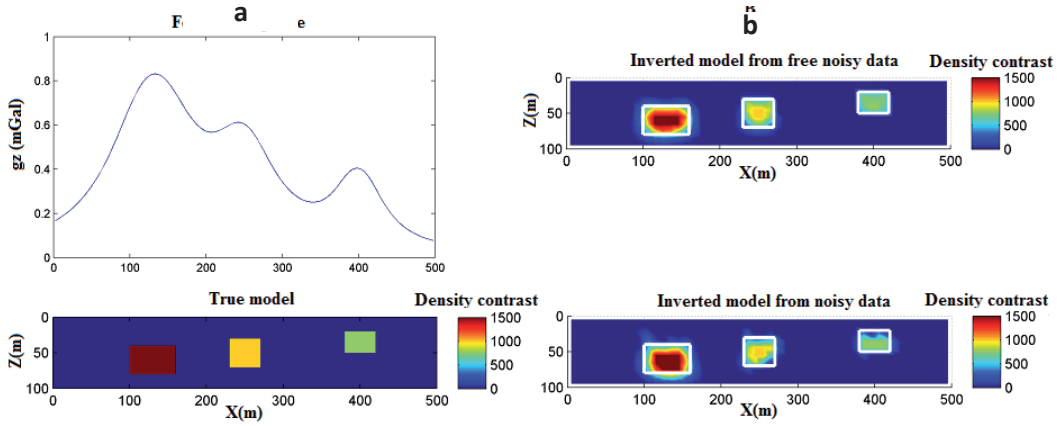

Fig. 5 - a) True model of three compact bodies with different density contrasts (kg/m³) and disparate depth ranges (bottom) and its associated forward response. b) Inversion sections derived from perfect (top) and noise contaminated data (bottom). For the deepest anomaly, the discrepancy between the results of noise free data and noisy data are not as much as the two other blocks because its size and density contrast are the largest ones leading to the largest gravity anomaly.

Table 6 - Inversion parameters for the multisource model.

Multisource model	Regularisation parameter	Depth weighting exponent	Number of iterations	Rms (%)
Noise free data	10^{-7}×MaxKer	2	4	2.57
Noisy data (2%)	10^{-1}×MaxKer	2	4	3.82

Overall, from these different synthetic cases, it can be deduced that the suggested inversion procedure: i) can handle different cases, ii) the efficiency of the flexible modified depth weighting function, which was presented by Cella and Fedi (2012), was also demonstrated, iii) the critical inversion parameters, like the regularisation parameter, can be chosen in the same manner even for different cases which may be related to the maximum value of the kernel matrix and iv) the results were encouraging enough to apply the inversion algorithm to the real data sets and investigate its performance in practical applications.

4. Model applications with real data

In order to examine the applicability of the inversion algorithm for practical implementations, two different field data sets are used.

4.1. Salt dome of Rogun (Tajikistan)

The first real data set is from the salt dome of a region near Rogun city in Tajikistan including rough topography where a dam is built. The main geological units of the interested area are: i) silt, mud, sandstone, granodiorite, conglomerate, and limestone from Cretaceous and ii) evaporites (gypsum and halite) from Triassic (OSHC Barki Tojik, 2012). The location of the area, including the microgravity network, can be seen on a Google Earth map, in Fig. 6. The complexity of the interpretation process is due to the proximity of the constituting material densities and very rough topography of the surrounding area. Since the borehole encountered a thick layer of gypsum with thin interbedded marlstone and claystone, a geological assumption about the presence of an evaporite dome was inferred.

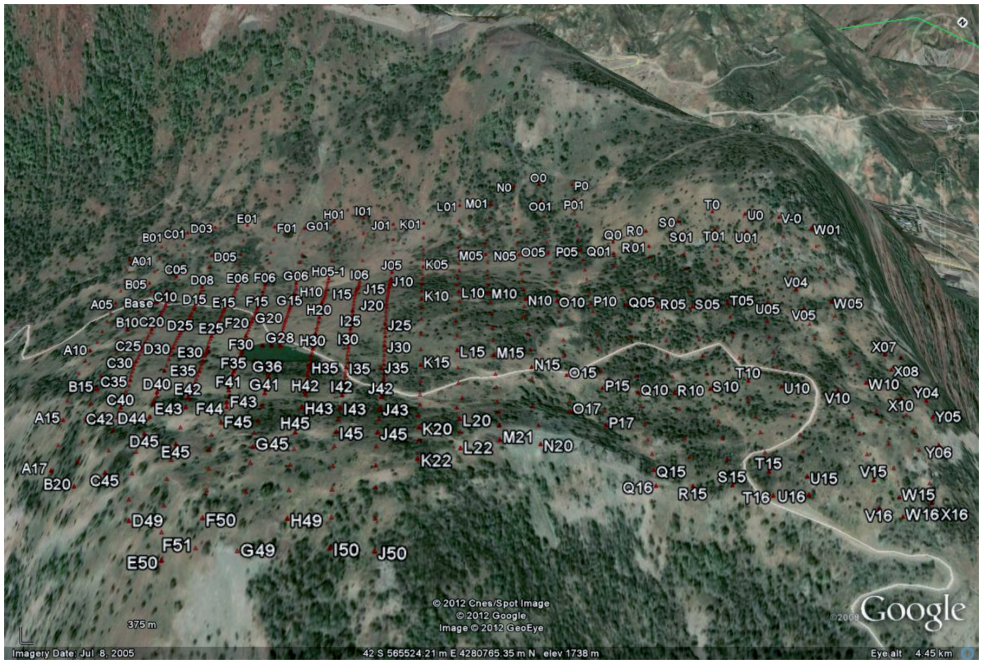

Fig. 6 - Site of the area including microgravity network in Google Earth map (Ardestani, 2014).

Data were collected by Scintrex CG3 gravimeter including 700 stations. Data sample intervals along the profiles were from 10 to 30 m, while distance between the profiles was 50 m. From removing the trend surface of degree 2, the residual anomalies are obtained (Fig. 7). Evaporites and their solution cavities produce negative anomalies, therefore, our focus is on the negative anomaly (anomalies) during the interpretation procedure. Fig. 7 represents several negative anomalies and here the main central one is investigated due to its closeness to the borehole DZ2, for which the depths of the encountered deposits in the borehole can be found in Table 7.

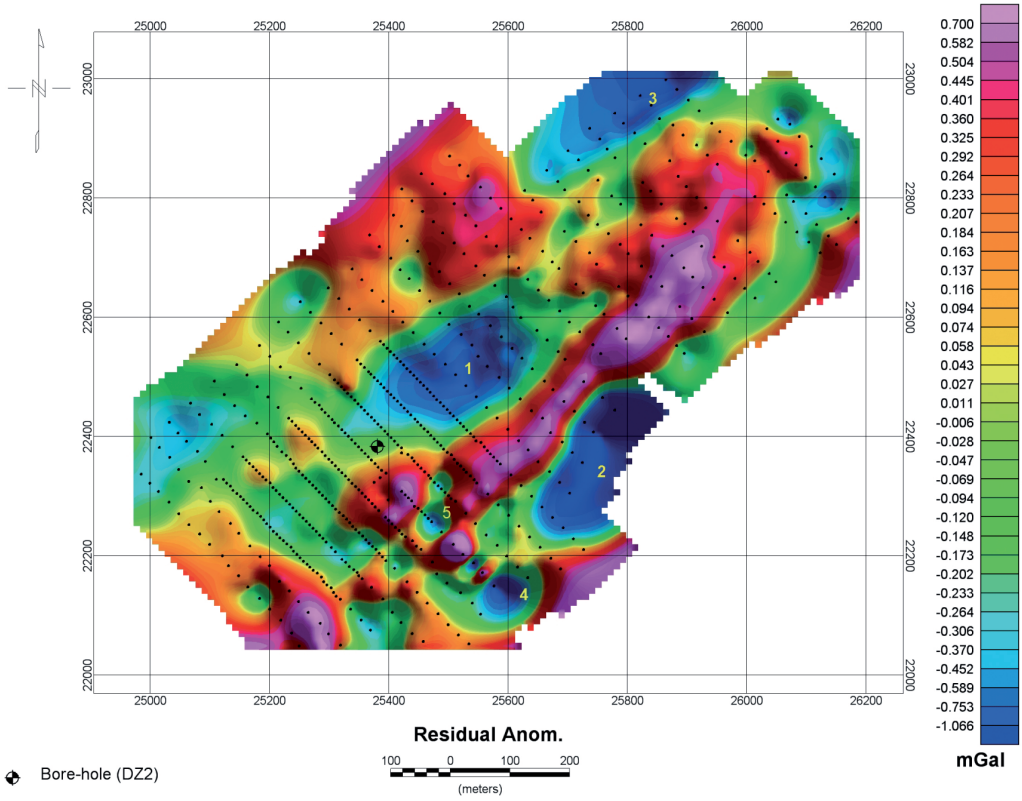

Fig. 7 - The residual anomalies by removing the trend surface of degree 2 (Ardestani, 2014). Here, the central anomaly 1 is of interest and the drilled borehole can be observed close to the anomaly 1. This borehole is drilled before microgravity data.

A profile of data with 10-m sample intervals was considered on the central negative anomaly (Fig. 8). There are two positive anomalies in both sides of the profile that are not investigated here. The subsurface is divided into 39 and 15 cells with the same horizontal and vertical lengths of 10 m. From *a priori* information, the lower and upper bounds of density contrast are -0.5 and 0.5 g/cm^3.

Table 7 - Borehole DZ2, which had been drilled before the microgravity survey was carried out (Ardestani, 2014).

Geological units	Depth ranges (m)
Overburden, clay with silt	0-68
Shaly limestone	68-74
Gypsum and claystone sequence	74-166

Fig. 9 displays the measured data and computed data from inversion model (top) and the inverse model (bottom). The retrieved model demonstrates a negative anomaly with the depth ranges from 20 to about 110 m and its horizontal extension is about 90 m. Minimum and maximum depth of the negative anomaly was obtained by Ardestani (2014) according to the Euler deconvolution and upward continuation techniques, respectively, being 20 and 120 m which supports the inversion result of the presented algorithm (Fig. 9).

From Table 7, it can be deduced that various geological units may generate this negative anomaly. Ardestani (2014) suggested two possibilities about the cause of the large low density anomaly: 1) salt masses and gypsum which are deeply rooted and influence the top layers as a dome and 2) the cavities and sink areas filled with clay in the overburden.

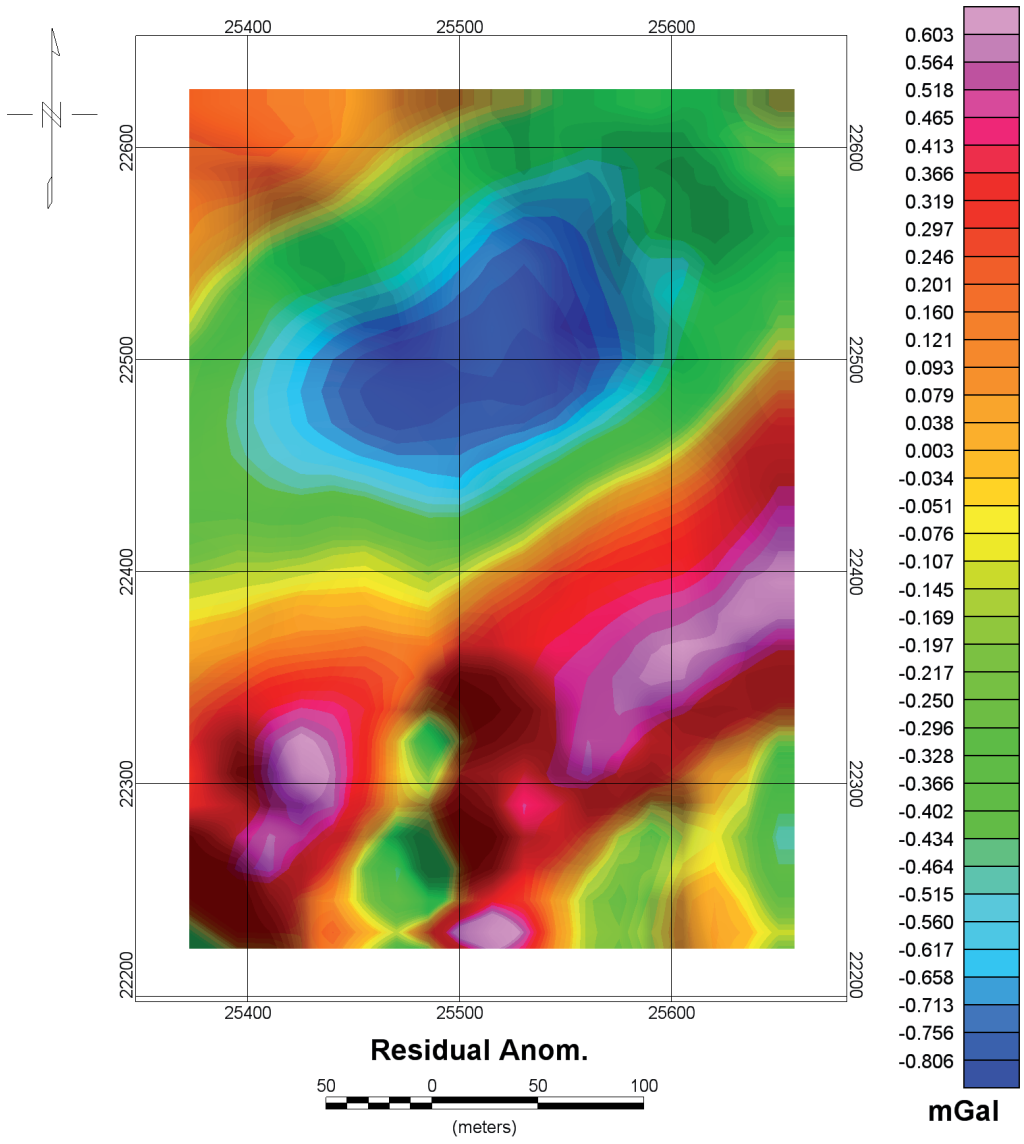

Fig. 8 - Central negative anomaly represented in Fig. 7 and the profile of interest of the data for 2D inversion are illustrated.

Returning to the main purpose of this paper, it should be noted that the regularisation parameter, depth weighting exponent, number of iterations and rms error of data misfit are 0.05×MaxKer, 2, 2, 6.35%, respectively. For real data, a value of 0.05×MaxKer is close enough to the optimum value of the regularisation parameter (10^{-1}×MaxKer) for the noisy synthetic data sets. This issue will be supported by the next real data case. Since an anomaly close to the sphere type was expected from *a priori* information, the exponent of depth weighting is considered to be 2. If the structural index is not known for a given data case, it can be obtained from Euler deconvolution or DEXP (Fedi, 2007) methods. The iterative inverse procedure is stopped after 2 iterations because significant improvement cannot be observed for larger values; furthermore, rms error of the data misfit increases.

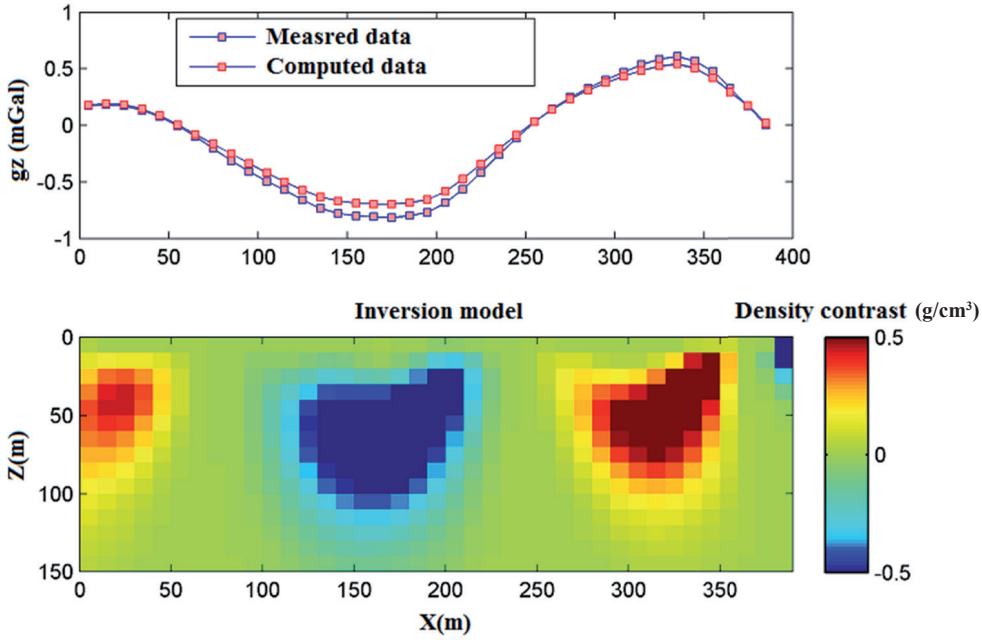

Fig. 9 - Measured data of the selected profile shown in Fig. 12 and calculated forward response derived from the inversion model (top). Inversion model derived from the considered profile (bottom).

4.2. Safo manganese mine data (Iran)

Another field data set considered to investigate the capability of the inversion algorithm is the Safo manganese mine in Iran. It is located in the NW of Iran, 25 km north of Chaldoran. This area is structurally and geologically located in the north-western Khoy ophiolite zone. The map of Iran and the geological map of the area are shown in Fig. 10. In the Khoy ophiolite zone, mineralogy is generally manganese, manganese-iron, iron, and manganese-iron-copper. Safo deposit ore has a simple mineralogical composition. Based on the previous studies, Pyroloic, Bixbite and Brownite are manganese ores in various parts of it, among which the dominant and abundant one in storage is Pyrolusite (Imamalipour, 2005).

The residual gravity anomaly map with the interested profile (black line) for 2D inversion is shown in Fig. 11. For inverting the data, subsurface is divided into 97 by 24 cells with horizontal

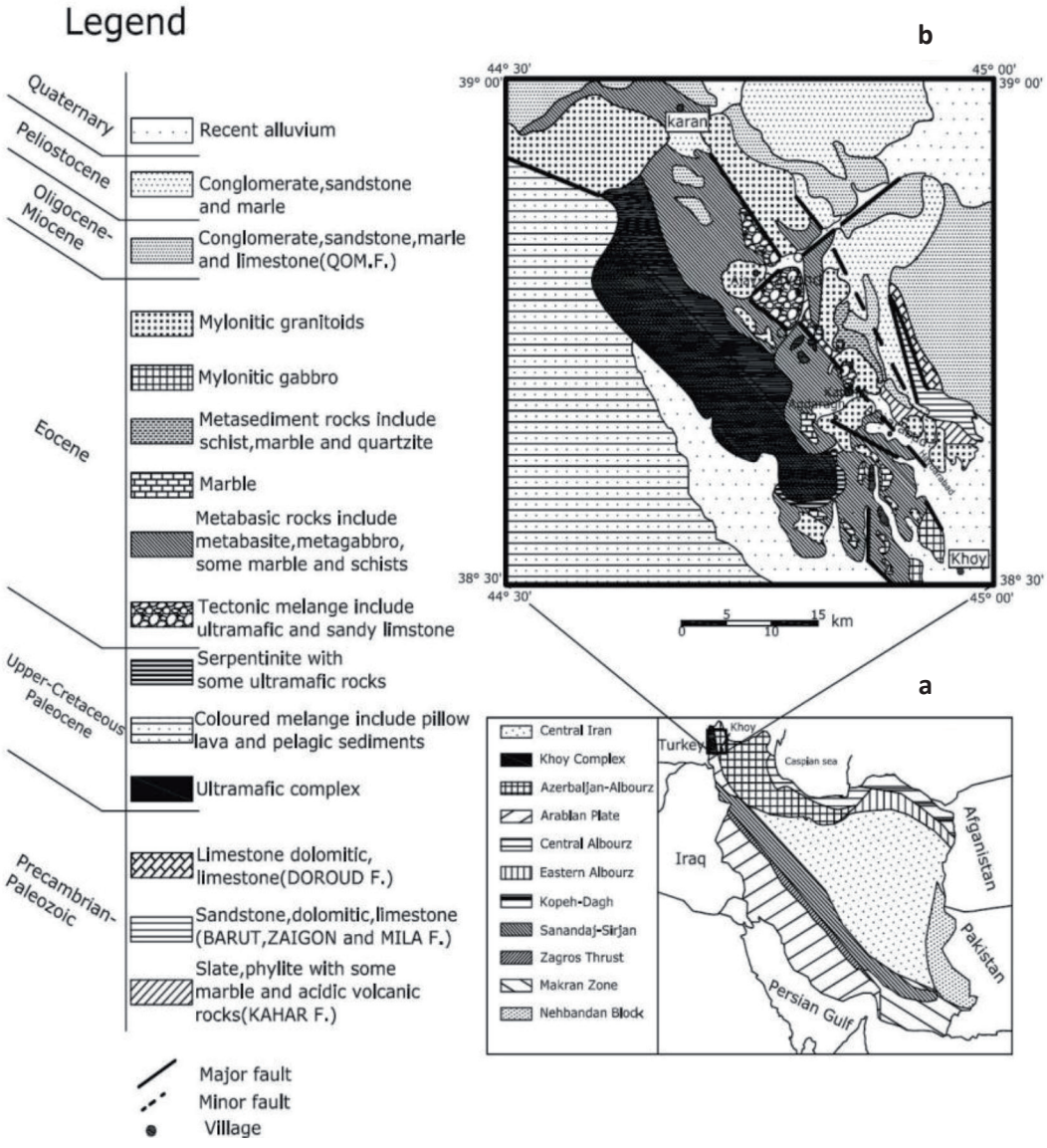

Fig. 10 - a) Iran map and b) geological map of the Khoy where the Safo manganese mine is situated (drawn from Azizi and Mohajel, 2007).

and vertical sizes of 2.5 m in *x* and *y* directions, respectively. The background density value was assumed to be 2.8 g/cm^3 and the attributed lower and upper bounds for density are 2.4 g/cm^3 and 4.8 g/cm^3. The recovered anomaly shows an anomalous compact body extending vertically from 2.5 to 25 m and its horizontal extension in the thickest part is 30 m (Fig. 12b). This result is in good enough agreement with the bore-hole drilling results on the site, demonstrating the manganese ore with range depths from 3-4 to 25-30 m (Noorizadeh, 2010). The regularisation parameter, the exponent of depth weighting, number of iterations and the rms error of data misfit are 0.05×MaxKer, 2, 2, 2.01%, respectively, indicating that all inverse parameters are equal to the last real case.

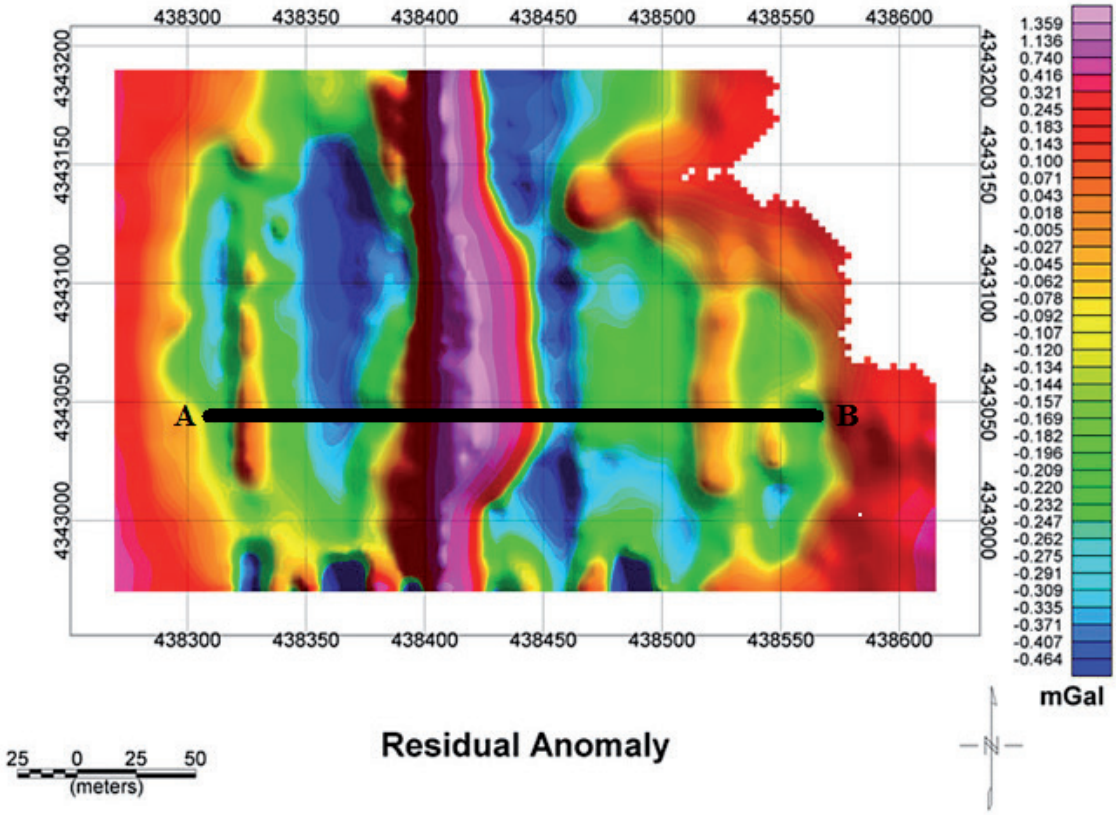

Fig. 11 - Residual gravity anomaly map with the profile of interest (black line) for 2D inversion.

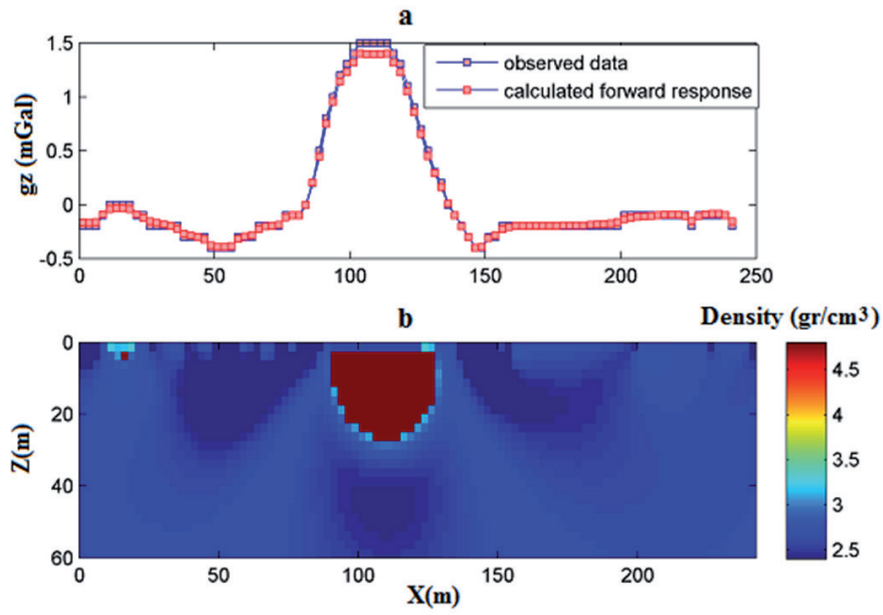

Fig. 12 - a) Measured data profile and computed data from inversion model shown in panel b; b) inversion model from the profile data set of the manganese mine of Safo representing an anomaly from near surface to about 25 m.

5. Conclusions

An inversion algorithm including a model weighting matrix, derived from multiplication of the compactness and the source type dependent depth weighting functions, is proposed. This weighting matrix is introduced in the weighted damped minimum length solution. We explicitly differentiated our algorithm from the focusing algorithm. Another original feature of this paper is the estimation of the regularisation parameter using the maximum value of the kernel matrix. Applying the suggested algorithm on different synthetic and real data sets enabled demonstrating its efficiency. The first synthetic case was a block anomaly placed in different depth ranges, the second one was a thin vertical dyke, and a multisource model, including different sized blocks with disparate depths to the top and density contrasts, was considered as a complex case for the third synthetic example. Finally, the inversion algorithm was applied to two real data sets from the salt dome in Tajikistan and a manganese mine in Iran.

The obtained results allowed drawing the following conclusions: i) for synthetic noise-free data, a regularisation parameter equal to 10^{-7}×MaxKer produces desirable inversion models; ii) the appropriate regularisation value for inversion of noise corrupted data and real data sets are 10^{-1}×MaxKer and 0.05×MaxKer, respectively, indicating no significant disparity between them; iii) the exponent of depth weighting should be picked according to the structural value of the source and our results support the efficacy of this flexible depth weighting function.

REFERENCES

Ardestani E.V.; 2014: *Detecting and modelling the evaporate dome in a dam site using microgravity data*. Boll. Geof. Teor. Appl., 55, 683-697.

Azizi H. and Mohajel M.; 2007: *Deformation in Tectonites in the northwest of Khoy*. J. Sci., 33, 65-73.

Barbosa V.C.F. and Silva J.B.C.; 1994: *Generalized compact gravity inversion*. Geophys., 59, 57-68.

Boulanger O. and Chouteau M.; 2001: *Constraint in 3D gravity inversion*. Geophys. Prospect., 49, 265-280.

Cella F. and Fedi M.; 2012: *Inversion of potential field data using the structural index as weighting function rate decay*. Geophys. Prospect., 60, 313-336.

Fedi M.; 2007: *DEXP: a fast method to determine the depth and the structural index of potential fields sources*. Geophys., 72, I1-I11.

FitzGerald D., Reid A. and McInerney P.; 2004: *New discrimination techniques for Euler deconvolution*. Comput. Geosci., 30, 461-469.

Guillen A. and Menichetti V.; 1984: *Gravity and magnetic inversion with minimization of a specific functional*. Geophys., 49, 1354-1360.

Hinze W.J.; 1990: *The role of gravity and magnetic methods in engineering and environmental studies: geotechnical and environmental*. Geotech. Environ. Geophys., 1, 75-126.

Ialongo S., Fedi M. and Florio G.; 2014: *Invariant models in the inversion of gravity and magnetic fields and their derivatives*. J. Appl. Geophys., 110, 51-62.

Imamalipour A.; 2005: *Geochemistry, mineralogy and origin of Safo manganese deposit*. In: Proc. 9th Meeting of Geological Society of Iran, Tehran, Iran, pp. 256-269.

Last B.J. and Kubik K.; 1983: *Compact gravity inversion*. Geophys., 48, 713-721.

Li Y. and Oldenburg D.W.; 1996: *3-D inversion of magnetic data*. Geophys., 61, 394-408.

Li Y. and Oldenburg D.W.; 1998: *3D inversion of gravity data*. Geophys., 63, 109-119.

Linsser H.; 1967: *Investigation of tectonics by gravity detailing*. Geophys. Prospect., 15, 480-515.

Meng Z., Li F., Xu X., Huang D. and Zhang D.; 2017: *Fast inversion of gravity data using the symmetric successive over-relaxation (SSOR) preconditioned conjugate gradient algorithm*. Expl. Geophys., 48, 294-304.

Menke W.; 2012: *Geophysical data analysis, discrete inverse theory*. Academic Press, London, UK, 293 pp.

Namaki L., Gholami A. and Hafizi M.A.; 2011: *Edge-preserved 2-D inversion of magnetic data: an application to the Makran arc-trench complex*. Geophys. J. Int., 184, 1058-1068.

Nettleton L.L.; 1976: *Gravity and magnetics in oil prospecting*. McGraw-Hill, New York, NY, USA, 480 pp.

Noorizadeh A.; 2010: *Geological report, bore-hole results of Safo manganese mine*. Spadana Mining Company, Esfahan, Iran, 12 pp.

Open Joint Stock Holding Company (OSHPC) Barki Tojik; 2012: *Techno-economic assessment study for Rogun hydroelectric construction project.* Dushanbe, Tajikistan, Report No. P.002378 RP 6, 16 pp.

Paoletti V., Ialongo S., Florio G., Fedi M. and Cella F.; 2013: *Self-constrained inversion of potential fields*. Geophys. J. Int., 195, 854-869.

Paterson N.R. and Reeves C.V.; 1985: *Applications of gravity and magnetic surveys: the state-of-the-art in 1985*. Geophys., 50, 2558-2594.

Pilkington M.; 1997: *3-D magnetic imaging using conjugate gradients*. Geophys., 62, 1132-1142.

Pilkington M.; 2009: *3D magnetic data-space inversion with sparseness constraints*. Geophys., 74, L7-L15.

Portniaguine O. and Zhdanov M.S.; 1999: *Focusing geophysical inversion images*. Geophys., 64, 874-887.

Portniaguine O. and Zhdanov M.S.; 2002: *3-D magnetic inversion with data compression and image focusing*. Geophys., 67, 1532-1541.

Reid A.B.; 2003: *Short note: Euler magnetic structural index of a thin bed fault*. Geophys., 68, 1255-1256.

Reid A.B., Allsop J.M., Granser H., Millett A.J. and Somerton I.W.; 1990: *Magnetic interpretation in three dimensions using Euler deconvolution*. Geophys., 55, 80-91.

Stavrev P.Y.; 1997: *Euler deconvolution using differential similarity transformations of gravity and magnetic anomalies*. Geophys. Prospect., 45, 207-246.

Tikhonov A.N. and Arsenin V.Y.; 1977: *Solutions of ill-posed problems.* Society for Industrial and Applied Mathematics, New York, NY, USA, 487 pp.

Varfinezhad R., Oskooi B. and Fedi M.; 2020: *Joint inversion of DC resistivity and magnetic data, constrained by cross gradients, compactness and depth weighting*. Pure Appl. Geophys., 177, 4325-4343.

Vatankhah S., Ardestani V.E. and Renaut R.A.; 2014: *Automatic estimation of the regularization parameter in 2D focusing gravity inversion: application of the method to the Safo manganese mine in the northwest of Iran*. J. Geophys. Eng., 11, 45001-45011.

Ward S.H.; 1990: *Geotechnical and environmental geophysics*. Society of Exploration Geophysicists, Tulsa, OK, USA, 389 pp.

Corresponding author: Ramin Varfinezhad
Institute of Geophysics, University of Tehran
Northern Karegar str., Tehran, Iran
Phone: +98 919 8203127; e-mail: ramin.varfi@ut.ac.ir